Numerical Heat Transfer, Part A: Applications: An International Journal of Computation and Methodology

Publication details, including instructions for authors and subscription information:
http://www.tandfonline.com/loi/unht20

Transient Analysis on Forced Convection Phenomena in a Fluid Valve Using Nanofluid

Rehena Nasrin [a] , Salma Parvin [a] , M. A. Alim [a] & Ali J. Chamkha [b]

[a] Department of Mathematics, Bangladesh University of Engineering and Technology, Dhaka, Bangladesh

[b] Manufacturing Engineering Department, The Public Authority for Applied Education and Training, Shuweikh, Kuwait

Version of record first published: 27 Sep 2012.

To cite this article: Rehena Nasrin, Salma Parvin, M. A. Alim & Ali J. Chamkha (2012): Transient Analysis on Forced Convection Phenomena in a Fluid Valve Using Nanofluid, Numerical Heat Transfer, Part A: Applications: An International Journal of Computation and Methodology, 62:7, 589-604

To link to this article: http://dx.doi.org/10.1080/10407782.2012.707060

Numerical Heat Transfer, Part A, 62: 589–604, 2012

ISSN: 1040-7782 print/1521-0634 online
DOI: 10.1080/10407782.2012.707060

Taylor & Francis
Taylor & Francis Group

TRANSIENT ANALYSIS ON FORCED CONVECTION PHENOMENA IN A FLUID VALVE USING NANOFLUID

Rehena Nasrin[1], Salma Parvin[1], M. A. Alim[1], and Ali J. Chamkha[2]

[1]*Department of Mathematics, Bangladesh University of Engineering and Technology, Dhaka, Bangladesh*

[2]*Manufacturing Engineering Department, The Public Authority for Applied Education and Training, Shuweikh, Kuwait*

A transient numerical study is conducted to investigate the transport mechanism of forced convection in a fluid valve filled with water-CuO nanofluid. The flow enters from one inlet at the left with uniform temperature and velocity T_i and U_i, respectively, but can leave the valve through two outlets at the right. The upper and lower boundaries of the valve are heated with constant temperature T_h, while the remaining walls are perfectly insulated. The numerical approach is based on the finite element technique with Galerkin's weighted residual simulation. Solutions are obtained for fixed Prandtl number ($Pr = 1.47$), Reynolds number ($Re = 100$), and solid volume fraction ($\phi = 5\%$). The streamlines, isotherm plots, flow rate and the local Nusselt number (Nu_{local}) at both heated phases, the average Nusselt number (Nu) for base fluid, and nanofluid with the variation of nondimensional time (τ) are presented and discussed. It is found that the rate of heat transfer in the fluid valve reduces for longer time periods.

1. INTRODUCTION

Nanofluid technology has emerged as a new enhanced heat transfer technique in recent years. Nanofluid is made by adding nanoparticles and a surfactant into a base fluid and can greatly enhance thermal conductivity and convective heat transfer. The diameters of nanoparticles are usually less than 100 nm, which improves their suspension properties.

Investigations on natural convection of water-based nanofluids are conducted by Ogut [1] and Das and Ohal [2]. Kumar et al. [3] found the significant heat transfer enhancement by the dispersion of nanoparticles in the base fluid. Contradictory results were reported by Putra et al. [4] based on experimental investigation in a cylindrical enclosure filled with water-Cu or water-Al_2O_3 nanofluids. They reported a systematic and definite deterioration in the heat transfer for the high Rayleigh numbers, and the degree of deterioration depended on the density and concentration of the nanoparticles. Santra et al. [5, 6] modeled the nanofluids as a non-Newtonian

Received 29 November 2011; accepted 11 June 2012.

Address correspondence to Rehena Nasrin, Department of Mathematics, Bangladesh University of Engineering and Technology, Dhaka 1000, Bangladesh. E-mail: rehena@math.buet.ac.bd

NOMENCLATURE

C_p	specific heat at constant pressure, $KJ\,kg^{-1}K^{-1}$	X, Y	nondimensional Cartesian coordinates
		α	thermal diffusivity, $m^2\,s^{-1}$
k	thermal conductivity, $Wm^{-1}\,K^{-1}$	β	thermal expansion coefficient, K^{-1}
L	length of the fluid valve, m	ϕ	solid volume fraction
Nu	Nusselt number	θ	nondimensional temperature
p	dimensional pressure, Nm^{-2}	μ	dynamic viscosity of the fluid, $Kg\,m^{-1}s^{-1}$
P	nondimensional pressure	ν	kinematic viscosity of the fluid, m^2s^{-1}
Pr	Prandtl number	ρ	density of the fluid, $Kg\,m^{-3}$
Re	Reynolds number	τ	dimensionless time
T	dimensional temperature, K		
t	dimensional time, s	**Subscripts**	
u, v	velocity components (ms^{-1}) along x, y directions, respectively	f	base fluid
		h	heated wall
U, V	dimensionless velocity components along X, Y directions, respectively	i	inlet state
		nf	water-CuO nanofluid
x, y	Cartesian coordinates, m	s	solid particle

fluid, and observed a systematic decrease of the heat transfer as the volume fraction of the nanofluids increased. The possible determining factors for the heat transfer reduction in nanofluids include the variations of the size, shape, and distribution of nanoparticles and uncertainties in the thermophysical properties of nanofluids. Most of the published articles are concerned with the analysis of natural convection heat transfer of nanofluids in square or rectangular enclosures. For example, Wong et al. [7], Abu-Nada and Oztop [8], Ghasemi and Aminossadati [9], Muthtamilselvan et al. [10], and Abu-Nada et al. [11].

In reality, forced convection in a differentially heated enclosure is a prototype of many industrial applications and has received considerable attention because of its applicability in various fields. The moderately concentrating solar energy collector is an important example involving fluid valve geometry. Because of its practical importance, transient forced convection in valve is of great interest of the phenomenon in many technological processes, such as the design of solar collectors, thermal design of buildings, air conditioning, and the cooling of electronic circuit boards. In recent years, modification of heat transfer in cavities due to the introduction of wavy wall(s) has received sustained attention. The study of transient forced convective flow in valve geometry is more difficult than that of commonly used enclosures.

Many studies have described the larruping behaviors of nanofluids, such as their effective thermal conductivity under static conditions and the convective heat transfer associated with fluid flow phenomena [12, 13]. Liu and Liao [14] studied the sorption and agglutination phenomenon of nanofluids on a plain heating surface during pool boiling. Dai et al. [12] and Chen et al. [15] investigated convective flow drag and heat transfer of CuO nanofluid in a small tube. Their results showed that the pressure drop of the nanofluid per unit length was greater than that of water. The pressure drop increased with the increasing weight concentration of nanoparticles. In the laminar flow region, the pressure drop had a linear relationship with the Re number, while in the turbulent flow region the pressure drop increased sharply with the increase of the Re number. The critical Re number became lower while the tube diameter

was smaller. The convective heat transfer was obviously enhanced by adding nanoparticles. The nanoparticle weight concentration and flow status were the main factors influencing the heat transfer coefficient: the heat transfer coefficient increased with the increasing weight concentration, and the enhancement of heat transfer in the turbulent flow region was greater than that in the laminar flow region. Wen and Ding [16] reported an experiment on the convective heat transfer of water–γ-Al_2O_3 nanofluid. Pfautsch [17] studied the characteristics, flow development, and heat transfer coefficient of nanofluids under laminar forced convection over a flat plate. He concluded that there was a significant increase in the heat transfer coefficient: about a 16% increase in the heat transfer coefficient for the water-based nanofluid, and about a 100% increase for the ethylene glycol-based nanofluid.

Very recently, Lin and Violi [18] studied the problem of natural convection heat transfer of nanofluids in a vertical cavity where the effects of nonuniform particle diameter and temperature on thermal conductivity were shown. Moreover, natural convection heat transfer in a nanofluid-filled trapezoidal enclosure was analyzed by Saleh et al. [19]. They found that acute sloping wall and Cu nanoparticles with high concentration were effective to enhance the rate of heat transfer. Raisi et al. [20] numerically studied the forced convection of laminar nanofluid in a microchannel with both slip and no-slip conditions. Their results indicated that the heat transfer rate was significantly affected by the solid volume fraction and slip velocity coefficients at high Reynolds number. Entropy generation due to natural convection in a partially open cavity with a thin heat source subjected to a nanofluid was performed by Mahmoudi et al. [21]. Here, the study had been carried out for a Rayleigh number in the range $10^3 < \mathrm{Ra} < 10^6$, and for solid volume fraction $0 < \phi < 0.05$. In order to investigate the effect of the heat source and open boundary location, six different configurations were considered.

Up to now, all the nanofluids in the existing research used a surfactant to help nanoparticle suspending. Due to the stickiness of the surfactant, the sedimentation on the tube wall became colloid and difficult to clear. The nanoparticles in the sedimentation could not suspend again. This kind of nanofluid would jam pipes during a prolonged period of operation. In order to overcome this disadvantage, recently, researchers used nanoparticle suspensions consisting of de-ionized water and nanoparticles without surfactant. During the flow process, the good suspension properties remained. So far, there is no research on the analysis of transient forced convective heat transfer on nanofluid in a fluid valve. Therefore, transient forced convection also becomes a crucial point of this study. The main issues discusse here are as follows: comparisons of the convective flow drag and heat transfer characteristics between pure water and water-CuO nanofluid in the fluid valve.

It's hoped that the theoretical prediction in this article is a useful guide for experimentalists to study the effectiveness of forced convection in a valve filled with nanofluid to increase the rate of heat transfer.

2. PHYSICAL CONFIGURATION

Figure 1 shows a schematic diagram of the fluid valve. The model describes a valve where it is possible to direct the flow into one of two channels. Flow of varying degrees can also occur in both channels during the opening and closing stages. Flow

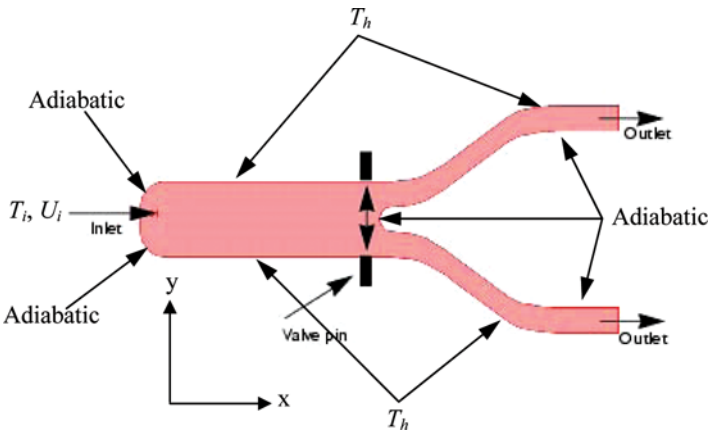

Figure 1. Depiction of the geometry and the operation of the fluid valve (color figure available online).

enters from one inlet at the left, but can leave the valve through two outlets at the right. The choice of outlet depends upon the position of the valve pin. In this model, two valve pins oscillate from in front of one outlet channel to being in front of the other. Sometimes flow is possible through both outlets, depending on the position of the pins. The valve pin moves according to a sinusoidal function of time. The inlet fluid velocity and temperature are U_i and T_i, respectivly. The upper and lower boundaries of the valve are heated with constant temperature T_h, while the remaining walls are perfectly insulated. The fluid in the valve is water-based nanofluid containing CuO nanoparticles.

3. MATHEMATICAL FORMULATION

In the present problem, it is considered that the flow is steady, two-dimensional, laminar, incompressible, and there is no viscous dissipation. The radiation effect is neglected. The governing equations under Boussinesq approximation are as follows.

$$\frac{\partial u}{\partial x}+\frac{\partial v}{\partial y}=0 \tag{1}$$

$$\rho_{nf}\left(\frac{\partial u}{\partial t}+u\frac{\partial u}{\partial x}+v\frac{\partial u}{\partial y}\right)=-\frac{\partial p}{\partial x}+\mu_{nf}\left(\frac{\partial^2 u}{\partial x^2}+\frac{\partial^2 u}{\partial y^2}\right) \tag{2}$$

$$\rho_{nf}\left(\frac{\partial v}{\partial t}+u\frac{\partial v}{\partial x}+v\frac{\partial v}{\partial y}\right)=-\frac{\partial p}{\partial y}+\mu_{nf}\left(\frac{\partial^2 v}{\partial x^2}+\frac{\partial^2 v}{\partial y^2}\right) \tag{3}$$

$$\frac{\partial T}{\partial t}+u\frac{\partial T}{\partial x}+v\frac{\partial T}{\partial y}=\alpha_{nf}\left(\frac{\partial^2 T}{\partial x^2}+\frac{\partial^2 T}{\partial y^2}\right) \tag{4}$$

where $\rho_{nf}=(1-\phi)\rho_f+\phi\rho_s$ is the density, $(\rho C_p)_{nf}=(1-\phi)(\rho C_p)_f+\phi(\rho C_p)_s$is the heat capacitance, $\beta_{nf}=(1-\phi)\beta_f+\phi\beta_s$ is the thermal expansion coefficient, $\alpha_{nf}=k_{nf}/\left(\rho C_p\right)_{nf}$ is the thermal diffusivity, $\mu_{nf}=\mu_f(1-\phi)^{-2.5}$is dynamic viscosity of the Brinkman model [22], and $k_{nf}=k_f\frac{k_s+2k_f-2\phi\left(k_f-k_s\right)}{k_s+2k_f+\phi\left(k_f-k_s\right)}$ is the thermal conductivity of the Maxwell Garnett (MG) model [23] of the nanofluid.

The boundary conditions are as follows.

At the upper and lower surfaces: $T=T_h$

At the inlet opening: $T=T_i$, $u=U_i$

At the remaining boundaries: $\frac{\partial T}{\partial n}=0$

At all solid boundaries: $u=v=0$

At the outlet opening convective boundary condition: $p=0$

The movement of the valve is described with an analytic expression *pin*, which returns the value of one in the area corresponding to the valve pin and zero elsewhere. This model describes a valve or a gate where flow can be directed into one of two channels. A large viscosity is specified in the region corresponding to the valve pin that in effect stops the flow in this region. A logical expression for the viscosity is introduced to simulate the movement of the valve pin. The viscosity is then expressed by $\mu_{nf}=\mu_f\,(1-\phi)^{-2.5}+pin.\,\mu_\infty$ where μ_f is the fluid viscosity, $\mu_\infty$is a very large viscosity (ideally infinite), and pin is described by $pin=x_{pin}y_{pin}$. Where $x_{pin}=(x>x_0)$ $(x<x_1)$, $y_{pin}=1-(y>y_1)+(y>y_2)$.

y_1 and y_2 depend on time, *t,* according to the following.

$$y_1=-y_0+y_{\max}\,Sin(2\pi t)$$

$$y_1=y_0+y_{\max}\,Sin(2\pi t)$$

and where y_0, x_0, x_1, and y_{max} are fixed in time and describe the size of the valve pin and the amplitude with which the pin moves.

The above equations are nondimensionalized by using the following dimensionless dependent and independent variables.

$X=\frac{x}{L}, Y=\frac{y}{L}, U=\frac{u}{U_i}, \tau=\frac{t}{U_i}, V=\frac{v}{U_i}, P=\frac{p}{\rho_f U_i^2}, \theta=\frac{T-T_i}{T_h-T_i}$

After substitution of the above variables into the Eqs. (1) – (4), we get the following nondimensional equations.

$$\frac{\partial U}{\partial X}+\frac{\partial V}{\partial Y}=0 \tag{5}$$

$$\frac{\partial U}{\partial \tau}+U\frac{\partial U}{\partial X}+V\frac{\partial U}{\partial Y}=-\frac{\rho_f}{\rho_{nf}}\frac{\partial P}{\partial X}+Pr\frac{\nu_{nf}}{\nu_f}\left(\frac{\partial^2 U}{\partial X^2}+\frac{\partial^2 U}{\partial Y^2}\right) \tag{6}$$

$$\frac{\partial V}{\partial \tau}+U\frac{\partial V}{\partial X}+V\frac{\partial V}{\partial Y}=-\frac{\rho_f}{\rho_{nf}}\frac{\partial P}{\partial Y}+Pr\frac{\nu_{nf}}{\nu_f}\left(\frac{\partial^2 V}{\partial X^2}+\frac{\partial^2 V}{\partial Y^2}\right) \tag{7}$$

$$\frac{\partial\theta}{\partial\tau}+U\frac{\partial\theta}{\partial X}+V\frac{\partial\theta}{\partial Y}=\frac{1}{Re\,Pr}\left(\frac{\partial^2\theta}{\partial X^2}+\frac{\partial^2\theta}{\partial Y^2}\right) \tag{8}$$

where $\mathrm{Pr}=\frac{\nu_f}{\alpha_f}$ is the Prandtl number and $\mathrm{Re}=\frac{U_i L}{\nu_f}$ is the reynolds number.

The corresponding boundary conditions then take the following form.

At the upper-lower boundaries: $\theta=1$

At the inlet: $\theta=0$, $U=1$

At the outlet: convective boundary condition $P=0$

At remaining boundaries: $\frac{\partial\theta}{\partial N}=0$ At all solid boundaries $U=V=0$

The local Nusselt number at the heated surface of the valve may be expressed as follows.

$$\mathrm{Nu}_{local}=-\left(\frac{k_{nf}}{k_f}\right)\frac{\partial\theta}{\partial N}$$

The average Nusselt number takes the following form

$$Nu=\frac{1}{S}\int_0^S Nu_{local}\,dS$$

where $\frac{\partial\theta}{\partial N}=\sqrt{\left(\frac{\partial\theta}{\partial X}\right)^2+\left(\frac{\partial\theta}{\partial Y}\right)^2}$ and S, N are the nondimensional length and coordinate along the heated surface, respectively.

4. NUMERICAL TECHNIQUE

The Galerkin finite element method [24, 25] is used to solve the nondimensional governing equations along with boundary conditions for the considered problem. The equation of continuity has been used as a constraint due to mass conservation, and this restriction may be used to find the pressure distribution. The penalty finite element method [26] is used to solve Eqs. (2) – (4), where the pressure P is eliminated by a penalty constraint. The continuity equation is automatically fulfilled for large values of this penalty constraint. then, the velocity components (U, V), and temperature (θ) are expanded using a basis set. The Galerkin finite element technique yields the subsequent nonlinear residual equations. Three points Gaussian quadrature is used to evaluate the integrals in these equations. The nonlinear residual equations are solved using Newton–Raphson method to determine the coefficients of the expansions. The convergence of solutions is assumed when the relative error for each variable between consecutive iterations is recorded below the convergence criterion ϵ, such that $|\psi^{n+1}-\psi^n|\leq 10^{-4}$, where n is the number of iteration and Ψ is a function of U, V, and θ.

4.1. Grid Refinement Test

In order to determine the proper grid size for this study, a grid independence test is conducted with five types of mesh for $\mathrm{Pr}=6.62$, $\mathrm{Re}=100$, and $\phi=5\%$. The

Table 1. Grid sensitivity check at $Pr = 6.62$, $Re = 100$ and $\phi = 5\%$

Nodes (elements)	3,224 (2,569)	5,982 (4,730)	8,538 (6,516)	12,666 (8,657)	20,524 (10,426)
Nu	5.52945	7.98176	9.18701	9.6566249	9.7666249
Time (s)	226.265	292.594	388.157	421.328	627.375

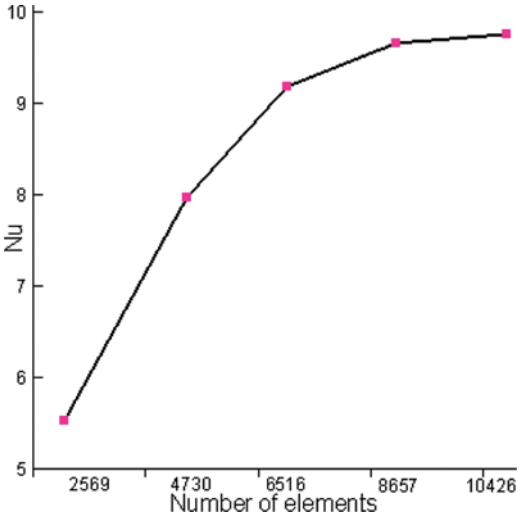

Figure 2. Grid independency study for $Pr = 6.62$, $Re = 100$, and $\phi = 5\%$ (color figure available online).

extreme value of Nu is used as a sensitivity measure of the accuracy of the solution and is selected as the monitoring variable.

Considering both the accuracy of numerical value and computational time, the present calculations are performed with 12,666 nodes and an 8,657 elements grid system. This is described in Table 1 and Figure 2.

4.2. Thermophysical Properties

The thermophysical properties of fluid (water) and solid CuO are tabulated in Table 2. The properties are taken from reference [27].

Table 2. Thermo-physical properties of water-CuO nanofluid

Physical properties	Water	CuO
C_p	4,182	540
ρ	998.1	6,510
K	0.6	18
$\alpha \times 10^7$ (m^2/s)	1.47	57.45
β	2.2×10^{-4}	8.5×10^{-6}

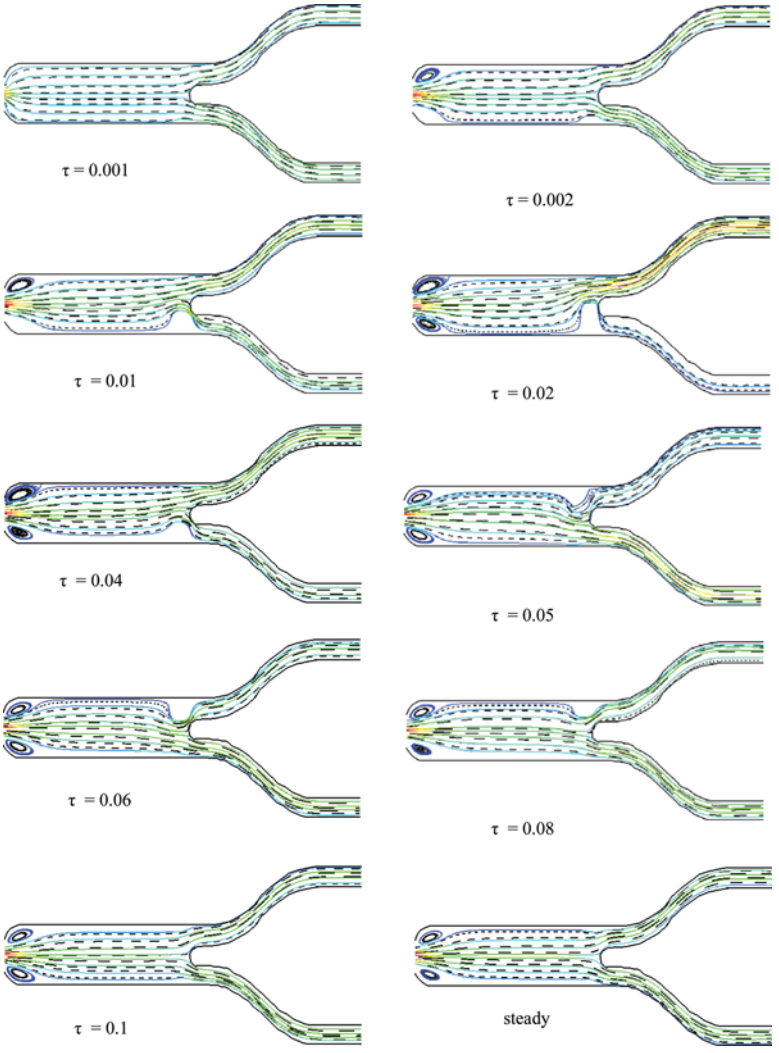

Figure 3. Transient behavior of streamlines at Re = 100 and Pr = 6.62. (Solid lines for nanofluid and dashed lines for base fluid.) (color figure available online).

4.3. Code Validation

The present numerical code is validated in the author's previous work [28], which is not repeated here.

5. RESULTS AND DISCUSSION

In this section, numerical results in terms of streamlines and isotherms for transient analysis are displayed, while Reynolds number Re, Prandtl number, Pr and solid volume fraction ϕ are fixed at 100, 6.62 and 5%, respectively. In addition,

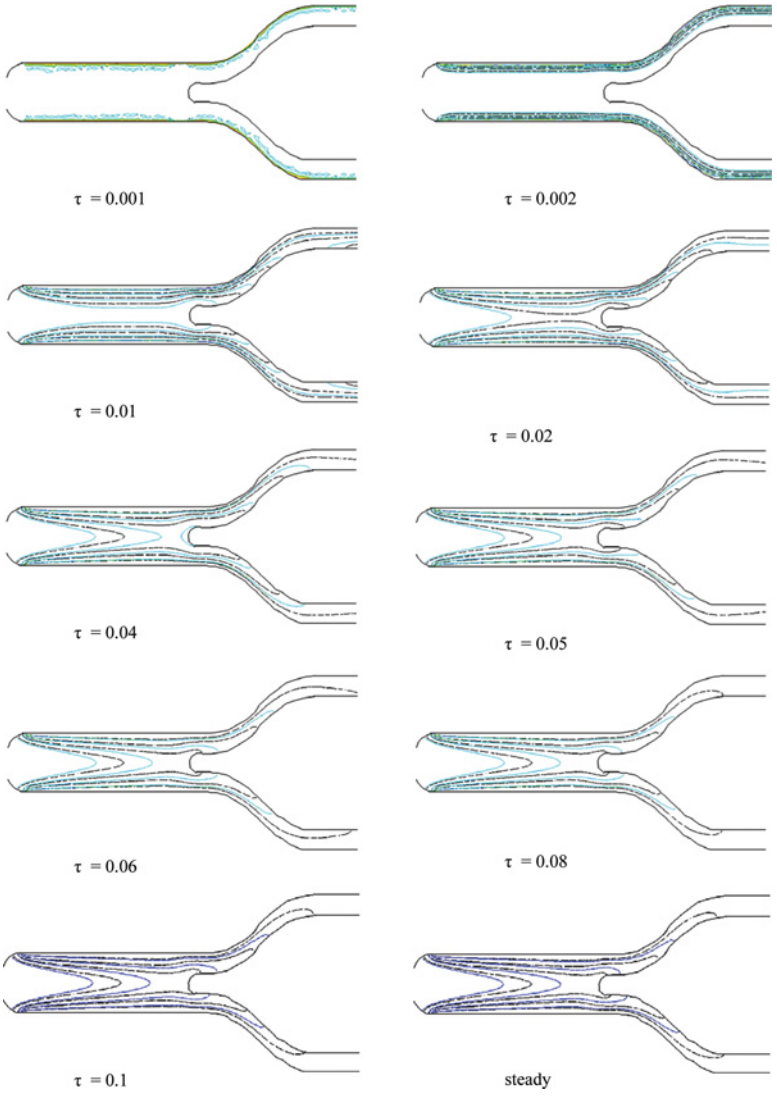

Figure 4. Transient behavior of isotherms at Re = 100 and Pr = 6.62. (Solid lines for nanofluid and dashed lines for base fluid.) (color figure available online).

the values of the local and average Nusselt number, average bulk temperature, V-velocity at a particular point, velocity field and flow rate with time have been calculated for both water and water-CuO nanofluid.

5.1. Velocity Field

The velocity field (modulus of the velocity vector) when the valve is completely open is displayed in Figure 3. First, the plot shows that the inlet is smaller than the compartment that it enters, so that some distance is required before the flow reaches

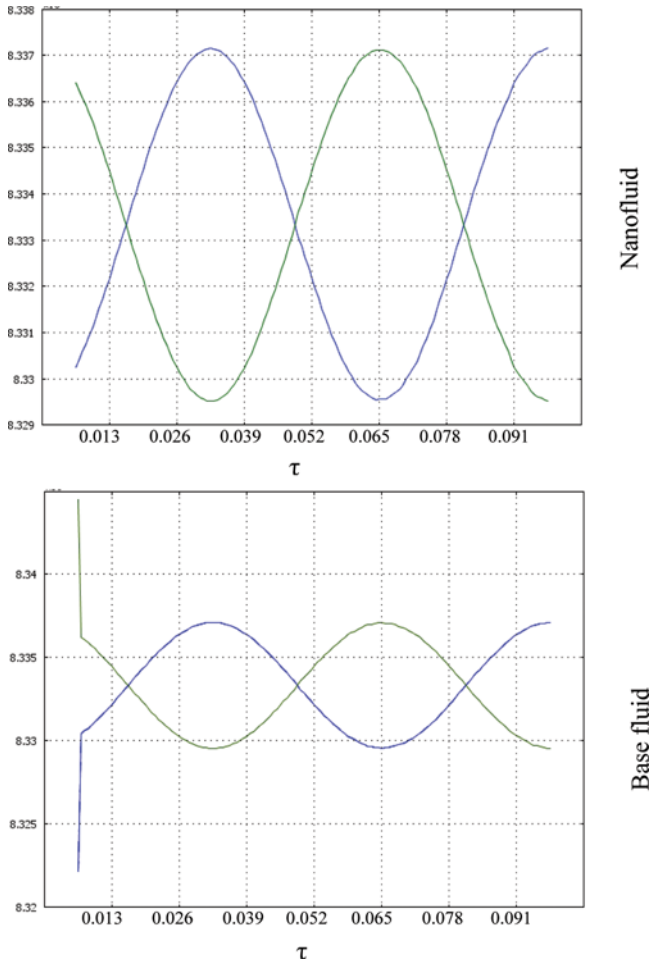

Figure 5. The blue line shows flow rate in the upper branch as a function of time, while the green line shows the flow rate in the lower branch (color figure available online).

another parabolic profile for the main body of the inlet chamber. In the velocity vector, some recirculation occurring at the corners of the chamber beside the inlet is visible. Second, the structure of the outlet channels leads to a slight thinning toward the middle of the channels. This provides a slight acceleration, and subsequentl, greater velocity magnitude in these regions.

The occurring nondimensional time of undershoot is chosen as the measure for the development time of the convective flow. Figure 3 presents the flow development as a function of time that is used for the cases of nanofluid and base fluid. The time instant for undershoot is decreased, while the trough value is increased with increasing time. At higher time, the development of flow is nearly identical for both types of fluids. The deviation slightly grows as the time is decreased, such that in the case of nanofluid the flow always takes the longest time to develop. As shown in Figure 3, initially the

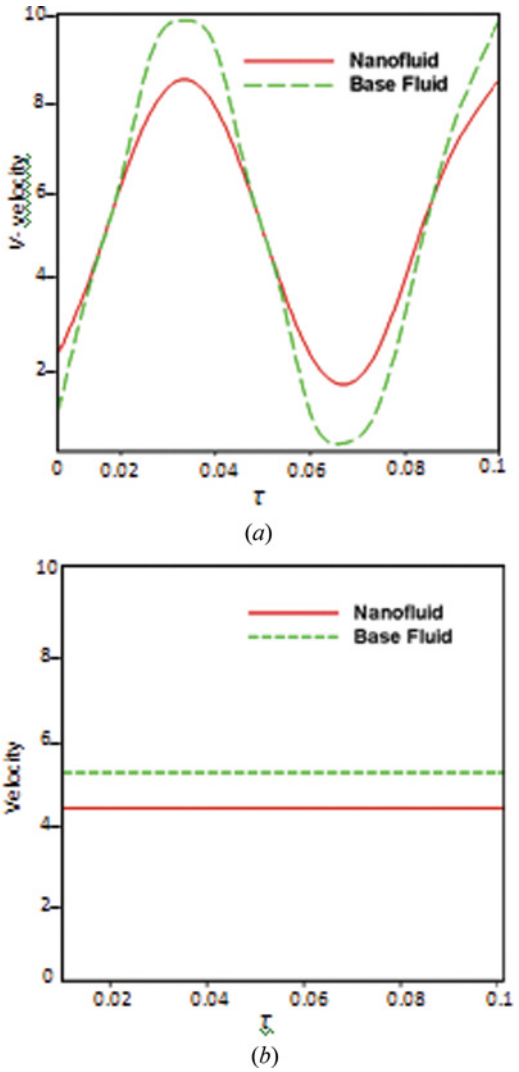

Figure 6. Plots of (*a*) *V*-velocity at the point (0.006, 0) in the valve, and (*b*) velocity as a function of time (color figure available online).

flow is laminar that is inflow and enters from the left and exits from the upper and the lower phase of the fluid valve. Due to increasing time, two tiny vortices are created near the opening inlet. In addition, velocity field changes its pattern near the lower to upper position of the valve pin. Finally, at time $\tau \geq 0.1$ the flow becomes steady.

5.2. Temperature Field

The thermal development as a function of time used for both water- CuO nanofluid and clear water is depicted in Figure 4. At the primary stage of time, the thermal current activities are identical for both fluids. The isotherms are

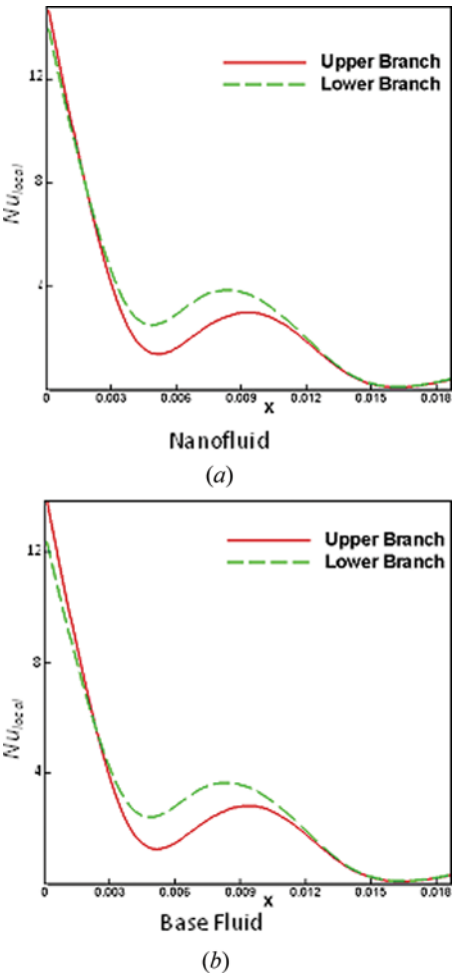

Figure 7. Plots of (*a*) Nu_{local} for nanofluid, and (*b*) Nu_{local} for base fluid (color figure available online).

clustered near the upper and lower hot surfaces. The deviation slightly grows as the time is increased, such that in the case of clear water the thermal field always takes the longest time to develop a thermal boundary layer near the heated surfaces. Sequentially, the isotherms dissipated from the heated boundaries and occupy the bulk of the fluid valve. The thermal plume develops at the inlet rapidly for nanofluid, whereas it takes time for the base fluid. This is due to the fact that inertia force enhances fluid velocity near the inlet position. After time $\tau = 0.1$, there is no variation in the isothermal lines, so that a steady state pattern is observed.

5.3. Flow Rate

Figure 5 shows a plot of the flow rates (integral of the velocity vector over the outlets) in the upper and lower channels. For both nanofluid and pure water, the

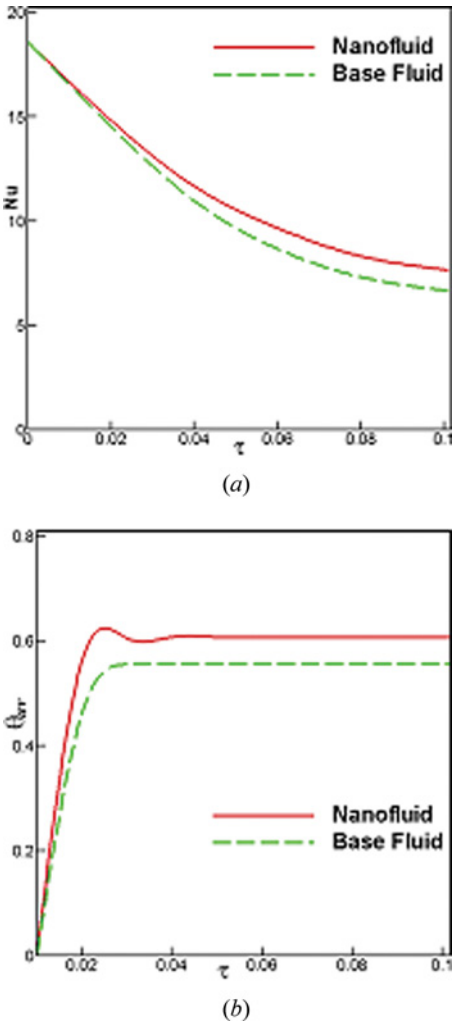

Figure 8. Plots of (*a*) average Nusselt number, and (*b*) average temperature in transient analysis (color figure available online).

figure illustrates the periodic flow due to the periodic motion of the valve pin. The results predicted by neglecting the Brownian motion effects are compared with those obtained by taking the Brownian motion effects into consideration.

The velocity in the vertical direction at a perticular point (0.006, 0) in the valve and subdomain velocity as a function of time are illustrated in Figure 6*a* and 6*b*. It is seen that the *V*-velocity is a sinusoidal pattern because of the periodic movement of the valve pin. The wave amplitude for clear water is found greater than the water-CuO nanofluid; but the subdomain velocity is uniform all over the domain for both kinds of fluids, whereas the base fluid has higher velocity compared to the nanofluid.

5.4. Heat Transfer

In the present study, the local Nusselt number (Nu_{local}) along with the X-axis for both nanofluid (with $\phi = 0.05$) and clear water are presented in Figures 7*a* and *b*. With increasing X, the local Nusselt number decreases due to decrement of temperature difference and increment of thickness of boundary layer for both types of fluids. The local Nusselt number becomes relative maximum at the peaks, which results in increment of compression of isotherms.

The time-averaged Nusselt number is obtained by computing the time average of the average Nusselt number over the hot surfaces for a process given by total time being the duration of the process of interest. Figure 8(*a*) expresses that the average Nusselt number decreases with higher time for both cases, whereas the nanofluid has greater heat transfer rate than the base fluid. In order to reach steady state, a situation rate of heat transfer reduces by 58% and 64% for nanofluid and basefluid, respectively. It is observed in Figure 8 *b* that the average fluid temperature increases for rising values of time up to $\tau \leq 0.03$. Then, it is almost identical with the variation of time. Initially, bulk temperature of both fluids is the same but variation is observed within them with rising dimensionless time, where a higher temperature is found for nanofluid.

6. CONCLUSION

The problem of transient analysis on forced convection heat transfer in a valve filled with water-CuO nanofluid has been studied numerically. Flow and temperature field in terms of streamlines and isotherms have been considered for various dimensionless time until steady state observed. The results of the numerical analysis lead to the following conclusions.

- The structure of the fluid flow and temperature field within the fluid valve is found to be significantly dependent upon the time (τ).
- Heat transfer rate diminishes by 58% and 64% for nanofluid and basefluid, respectively, to reach steady state.
- The CuO nanoparticles are established to be most effective in enhancing performance of the heat transfer rate.
- The mean temperature of the fluid in the fluid valve increase with dimensionless time. In comparison, water-CuO nanofluids achieve a higher temperature than the base fluid.

Overall, the analysis also defines the operating range where water-CuO nanofluid can be considered effectively in determining the level of heat transfer augmentation.

REFERENCES

1. E. B. Ogut, Natural Convection of Water-Based Nanofluids in an Inclined Enclosure with a Heat Source, *Int. J. of Therm. Sci.*, vol. 48, pp. 2063–2073, 2009.

2. M. K. Das and P. S. Ohal, Natural Convection Heat Transfer Augmentation in a Partially Heated and Partially Cooled Square Cavity Utilizing Nanofluids, *Int. J. of Numer. Methods for Heat & Fluid Flow*, vol. 19, no. 1, pp. 411–431, 2009.
3. S. Kumar, S. K. Prasad and J. Banerjee, Analysis of Flow and Thermal Field in Nanofluid using a Single Phase Thermal Dispersion Model, *Appl. Math. Modelling*, vol. 34, pp. 573–592, 2009.
4. N. Putra and W. Roetzel, S. K. Das, Natural Convection of Nano-Fluids, *Heat and Mass Transfer*, vol. 39, pp. 775–78, 2003.
5. A. K. Santra, S. Sen, and N. Chakraborty, Study of Heat Transfer Characteristics of Copper–Water Nanofluid in a Differentially Heated Square Cavity with Different Viscosity Models, *J. of Enhanced Heat Transfer*, vol. 15, no. 4, pp. 273–287, 2008.
6. A. K. Santra, S. Sen, N. Chakraborty, Study of Heat Transfer Augmentation in a Differentially Heated Square Cavity using Copper–Water Nanofluid, *Int. J. of Therm. Sci.*, vol. 47, pp. 1113–1122, 2008.
7. K. F. V. Wong, B. L. Bon, S. Vu, and S. Samedi, Study of Nanofluid Natural Convection Phenomena in Rectangular Enclosures, *ASME Int. Mech. Eng. Cong. Exposition, Proc.* vol. 6, pp. 3–13, 2008.
8. E. Abu-Nada, and H. F. Oztop, Effects of Inclination Angle on Natural Convection in Enclosures Filled with Cu–Water Nanofluid, *Int. J. for Heat & Fluid Flow*, vol. 30, pp. 669–678, 2009.
9. B. Ghasemi and S. M. Aminossadati, Natural Convection Heat Transfer in an Inclined Enclosure Filled with a Water–CuO Nanofluid, *Numer. Heat Transfer. A.*, vol. 55, pp. 807–823, 2009.
10. M. Muthtamilselvan, P. Kandaswamy, and J. Lee, Heat Transfer Enhancement of Copper–Water Nanofluids in a Lid-Driven Enclosure, *Comm. in Nonlinear Sci. and Nume. Simulation*, vol. 15, no. 6, pp. 1501–1510, 2009.
11. E. Abu-Nada, Z. Masoud, H. F. Oztop, and A. Campo, Effect of Nanofluid Variable Properties on Natural Convection in Enclosures, *Int. J. of Therm. Sci.*, vol. 49, pp. 479–491, 2009.
12. W. T. Dai, J. M. Li, X. Chen, and B. X. Wang, Experimental Investigation on Convective Heat Transfer of Copper Oxide Nanoparticle Suspensions Inside Mini-Diameter Tubes, *J. Eng. Thermophysics*, vol. 24, no. 4, pp. 633–636, 2003.
13. W. T. Dai, J. M. Li, B. X. Wang, and X. Chen, An Experimental Study on the Flow and Heat Transfer Characteristics of Copper Oxide Nanoparticle Suspensions Inside Mini-Diameter Tube, *Ind. Heating*, vol. 5, pp. 1–4, 2002.
14. Z. H. Liu and L. Liao, Sorption and Agglutination Phenomenon of Nanofluids on a Plain Heating Surface during Pool Boiling, *Int. J. of Heat and Mass Transfer*, vol. 51, no. 5, 9–10, pp. 2593–2602, 2008.
15. X. Chen, J. M. Li, W. T. Dai, and B. X. Wang, Enhancing Convection Heat Transfer in Mini Tubes with Nanoparticle Suspensions, *J. Eng. Thermophysics*, vol. 25, no. 4, pp. 643–645, 2004.
16. D. S. Wen and Y. L Ding, Experimental Investigation into Convective Heat Transfer of Nanofluids at Entrance Area under Laminar Flow Region, *Int. J. of Heat and Mass Transfer*, vol. 47, pp. 5181–5188, 2004.
17. E. Pfautsch, Forced Convection in Nanofluids over a Flat Plate, M.Sc. Thesis, Faculty of the Graduate School, University of Missouri, Columbia, 2008.
18. K. C. Lin and Angela Violi, Natural Convection Heat Transfer of Nanofluids in a Vertical Cavity: Effects of Non-Uniform Particle Diameter and Temperature on Thermal Conductivity, *Int. J. of Heat and Fluid Flow*, vol. 31, pp. 236–245, 2010.
19. H. Saleh, R. Roslan, and I. Hashim, Natural Convection Heat Transfer in a Nanofluid-Filled Trapezoidal Enclosure, *Int. J. of Heat and Mass Transfer*, vol. 54, pp. 194–201, 2011.

20. A. Raisi, B. Ghasemi, and S. M. Aminossadati, A Numerical Study on the Forced Convection of Laminar Nanofluid in a Microchannel with Both Slip and No-Slip Conditions, *Numer. Heat Transfer A.*, vol. 59, no. 2, pp. 114–129, 2011.
21. A. H. Mahmoudi, M. Shahi, and F. Talebi, Entropy Generation Due to Natural Convection in a Partially Open Cavity with a Thin Heat Source Subjected to a Nanofluid, *Numer. Heat Transfer A.*, vol. 61, no. 4, pp. 283–305, 2012.
22. H. C. Brinkman, The Viscosity of Concentrated Suspensions and Solution, *J. Chem. Physics*, vol. 20, pp. 571–581, 1952.
23. J. C. Maxwell-Garnett, Colours in Metal Glasses and in Metallic Films, *Philos. Trans. Roy. Soc. A* vol. 203, pp. 385–420, 1904.
24. C. Taylor, and P. Hood, A Numerical Solution of the Navier-Stokes Equations using Finite Element Technique, *Computer and Fluids*, vol. 1, pp. 73–89, 1973.
25. P. Dechaumphai, *Finite Element Method in Engineering*, 2nd ed., Chulalongkorn University Press, Bangkok, P. R. China, 1999.
26. T. Basak, S. Roy, and I. Pop, Heat Flow Analysis for Natural Convection within Trapezoidal Enclosures based on Heatline Concept, *Int. J. of Heat and Mass Transfer*, vol. 52, pp. 2471–2483, 2009.
27. Z.-T. Yu, X. Xu, Y.-C. Hu, L.-W. Fan, and K.-F. Cen, Numerical Study of Transient Buoyancy-Driven Convective Heat Transfer of Water-Based Nanofluids in a Bottom-heated isosceles triangular enclosure, *Int. J. of Heat and Mass Transfer*, vol. 54, pp. 526–532, 2011.
28. R. Nasrin, Influences of Physical Parameters on Mixed Convection in a Horizontal Lid-Driven Cavity with an Undulating Base Surface, *Numer. Heat Transfer A.*, vol. 61, no. 4, pp. 306–321, 2012.